

Research Report - Four-Wave Mixing Complete Parameter Numerical Gain Solver for Semiconductor Devices

Zihao Lin
Third-order Nonlinear Interaction

August 23, 2019

Copyright © 2019 Robin Lin

Contents

1	Introduction	3
2	Four-Wave Mixing	3
2.1	Origin of Four-Wave Mixing	3
2.2	Pulse-Propagation Equations	4
2.3	Non-degenerate FWM Coupled Amplitude Equations	4
2.4	Degenerate FWM Coupled Amplitude Equations	6
3	Four-wave Mixing Numerical Solver Specifications	7
3.1	Simulation Parameters	7
3.2	Simulation Structure	7
3.3	Split-Step Fourier Method (SSFM)	8
4	Non-degenerate FWM Simulation Results	8
4.1	Non-degenerate FWM Signal Wavelength Scan	8
4.2	Non-degenerate FWM - Changing Pump Power	9
4.3	Non-degenerate FWM - Changing Two-photon Absorption Coefficient	9
5	Degenerate FWM Simulation Results	10
5.1	Non-degenerate FWM Signal Wavelength Scan	10
5.2	Degenerate FWM - Changing Pump Power	12
5.3	Degenerate FWM - Changing Two-photon Absorption Coefficient	12
6	Conclusion and Discussion	12
	References	13

1 Introduction

The primary motivation behind this work is to develop the theoretical foundations that govern four-wave mixing (FWM), a χ^3 process, and to build a numerical simulation that solves the set of four coupled amplitude equations.

Conventionally, numerical solvers are only capable of simulating the effects of FWM in optical fibres and take into account fibre dispersion, self-phase modulation, and linear loss [1]. In this work, a numerical solver has been developed that can be used to simulate FWM in semiconductor devices, such as waveguides, and can not only account for dispersion, self-phase modulation, and linear loss, but also two-photon absorption, a process that is only present in semiconductors. In total, 16 different parameters can be varied. They include: Pump power, refractive index model for the semiconductor device, signal wavelength, linear loss parameter, self-phase modulation parameters, T_0 , laser repetition rate, device length, number of periods, number of steps along t , number of repetitions per material, number of steps along the z -direction, step length along t , third-order effective area, and pulse shape.

In this report, the theory governing four-wave mixing is presented, which includes the derivation of both the degenerate and non-degenerate coupled-amplitude equations. Then, the specifications of the numerical solver are discussed. Then, experiment results for a signal wavelength scan, pump power scan, as well as a two-photon absorption coefficient scan are presented for both the non-degenerate and degenerate processes.

2 Four-Wave Mixing

2.1 Origin of Four-Wave Mixing

The effects of parametric processes, such as four-wave mixing (FWM) and third-harmonic generation, arise due to the nonlinear polarization induced in the propagation medium. Nonlinear terms are introduced and their magnitudes are governed by the nonlinear susceptibilities. Third-order parametric processes in general involve the interaction between four optical waves. Consider four optical waves oscillating at angular frequencies $\omega_1, \omega_2, \omega_3$, and ω_4 polarized along the same x -axis. There are generally two FWM processes: one involving the transfer of energy shared between three photons to a single photon, and one involving the annihilation and the simultaneous creation of two pairs of photons.

In the first FWM process, the relationship between the angular frequencies is: $\omega_4 = \omega_1 + \omega_2 + \omega_3$. The three angular frequencies can be identical ($\omega_1 = \omega_2 = \omega_3$), which would lead to third-harmonic generation, or frequency conversion if $\omega_1 = \omega_2 \neq \omega_3$.

In the second FWM process, the relationship between the angular frequencies is: $\omega_3 + \omega_4 = \omega_1 + \omega_2$.

The phase-matching condition for the above processes is as follows: $\Delta k = k_3 + k_4 - k_1 - k_2 = (n_3\omega_3 + n_4\omega_4 - n_1\omega_1 - n_2\omega_2)/c = 0$.

2.2 Pulse-Propagation Equations

Fundamentally, in four-wave mixing, two strong pump waves at ω_1 transfer energy to two waves at ω_3 , and ω_4 , upshifted and downshifted in frequency. Furthermore, a weak signal at ω_3 can be injected into the two pump waves in order to achieve parametric amplification and the production of a new wave at ω_4 .

We can start by studying the wave equation with both the linear and nonlinear components:

$$\nabla^2 \mathbf{E} - \frac{1}{c^2} \frac{\partial^2 \mathbf{E}}{\partial t^2} = \mu_0 \frac{\partial^2 \mathbf{P}_L}{\partial t^2} + \mu_0 \frac{\partial^2 \mathbf{P}_{NL}}{\partial t^2} \quad (1)$$

The j^{th} electric field component propagating inside the fibre is given by:

$$E_j(\mathbf{r}) = F_j(x, y) A_j(z) \quad (2)$$

$F_j(x, y)$ is the spatial distribution of the fibre mode of the j^{th} field. The evolution of the slow-varying pulse envelope amplitude $A_j(z)$ for each component during propagation can be obtained by solving the set of coupled amplitude equations.

2.3 Non-degenerate FWM Coupled Amplitude Equations

We can now consider the most general form of four-wave mixing (non-degenerate). The following four coupled amplitude equations can be solved in order to get wave amplitudes.

$$\frac{dA_1}{dz} = \frac{in'_2\omega_1}{c} \left[\left(f_{11} |A_1|^2 + 2 \sum_{k \neq 1} f_{1k} |A_k|^2 \right) A_1 + 2f_{1234} A_2^* A_3 A_4 e^{i\Delta kz} \right] - \frac{\alpha_{0,1}}{2A_{eff,1}^{(3)}} A_1 |A_1|^2 \quad (3)$$

$$\frac{dA_2}{dz} = \frac{in'_2\omega_2}{c} \left[\left(f_{22} |A_2|^2 + 2 \sum_{k \neq 2} f_{2k} |A_k|^2 \right) A_2 + 2f_{2134} A_1^* A_3 A_4 e^{i\Delta kz} \right] - \frac{\alpha_{0,2}}{2A_{eff,2}^{(3)}} A_2 |A_2|^2 \quad (4)$$

$$\frac{dA_3}{dz} = \frac{in'_2\omega_3}{c} \left[\left(f_{33} |A_3|^2 + 2 \sum_{k \neq 3} f_{3k} |A_k|^2 \right) A_3 + 2f_{3412} A_1 A_2 A_4^* e^{-i\Delta kz} \right] - \frac{\alpha_{0,3}}{2A_{eff,3}^{(3)}} A_3 |A_3|^2 \quad (5)$$

$$\frac{dA_4}{dz} = \frac{in'_2\omega_4}{c} \left[\left(f_{44} |A_4|^2 + 2 \sum_{k \neq 4} f_{4k} |A_k|^2 \right) A_4 + 2f_{4312} A_1 A_2 A_3^* e^{-i\Delta kz} \right] - \frac{\alpha_{0,4}}{2A_{eff,4}^{(3)}} A_4 |A_4|^2 \quad (6)$$

We can now make several simplifications to the existing model. The overlap integral f_{ijkl} and f_{ij} can be approximated as $1/A_{\text{eff}}$. With this approximation, the prefactor $\frac{in'_2\omega_4}{c}$ can be combined with $1/A_{\text{eff}}$ to form a new pre-factor of $\frac{in'_2\omega_4}{cA_{\text{eff}}}$. This term is equivalent to i multiplied by the nonlinear parameter γ .

The new set of coupled amplitude equations are now:

$$\frac{dA_1}{dz} = i\gamma \left[\left(|A_1|^2 + 2 \sum_{k \neq 1} |A_k|^2 \right) A_1 + 2A_2^* A_3 A_4 e^{i\Delta kz} \right] - \frac{\alpha_{0,1}}{2A_{eff,1}^{(3)}} A_1 |A_1|^2 \quad (7)$$

$$\frac{dA_2}{dz} = i\gamma \left[\left(|A_2|^2 + 2 \sum_{k \neq 2} |A_k|^2 \right) A_2 + 2A_1^* A_3 A_4 e^{i\Delta kz} \right] - \frac{\alpha_{0,2}}{2A_{eff,2}^{(3)}} A_2 |A_2|^2 \quad (8)$$

$$\frac{dA_3}{dz} = i\gamma \left[\left(|A_3|^2 + 2 \sum_{k \neq 3} |A_k|^2 \right) A_3 + 2A_4^* A_1 A_2 e^{-i\Delta kz} \right] - \frac{\alpha_{0,3}}{2A_{eff,3}^{(3)}} A_3 |A_3|^2 \quad (9)$$

$$\frac{dA_4}{dz} = i\gamma \left[\left(|A_4|^2 + 2 \sum_{k \neq 4} |A_k|^2 \right) A_4 + 2A_3^* A_1 A_2 e^{-i\Delta kz} \right] - \frac{\alpha_{0,4}}{2A_{eff,4}^{(3)}} A_4 |A_4|^2 \quad (10)$$

The effects of group-velocity dispersion (GVD) can be included by making the following substitution [2]:

$$\frac{dA_j}{dz} \rightarrow \frac{\partial A_j}{\partial z} + \beta_{1j} \frac{\partial A_j}{\partial t} + \frac{i}{2} \beta_{2j} \frac{\partial^2 A_j}{\partial t^2} + \frac{1}{2} \alpha_j A_j \quad (11)$$

In this case, we are assuming that all four waves in FWM are polarized along a principle axis of a birefringent fibre. The resulting four equations include the effects of self-phase modulation (SPM), cross-phase modulation (XPM), dispersion, as well as two-photon absorption (TPA):

$$\frac{\partial A_1}{\partial z} + \beta_{11} \frac{\partial A_1}{\partial t} + \frac{i}{2} \beta_{21} \frac{\partial^2 A_1}{\partial t^2} + \frac{1}{2} \alpha_1 A_1 = i\gamma \left[\left(|A_1|^2 + 2 \sum_{k \neq 1} |A_k|^2 \right) A_1 + 2A_2^* A_3 A_4 e^{i\Delta kz} \right] - \frac{\alpha_{0,1}}{2A_{eff,1}^{(3)}} A_1 |A_1|^2 \quad (12)$$

$$\frac{\partial A_2}{\partial z} + \beta_{12} \frac{\partial A_2}{\partial t} + \frac{i}{2} \beta_{22} \frac{\partial^2 A_2}{\partial t^2} + \frac{1}{2} \alpha_2 A_2 = i\gamma \left[\left(|A_2|^2 + 2 \sum_{k \neq 2} |A_k|^2 \right) A_2 + 2A_1^* A_3 A_4 e^{i\Delta kz} \right] - \frac{\alpha_{0,2}}{2A_{eff,2}^{(3)}} A_2 |A_2|^2 \quad (13)$$

$$\frac{\partial A_3}{\partial z} + \beta_{13} \frac{\partial A_3}{\partial t} + \frac{i}{2} \beta_{23} \frac{\partial^2 A_3}{\partial t^2} + \frac{1}{2} \alpha_3 A_3 = i\gamma \left[\left(|A_3|^2 + 2 \sum_{k \neq 3} |A_k|^2 \right) A_3 + 2A_4^* A_1 A_2 e^{-i\Delta kz} \right] - \frac{\alpha_{0,3}}{2A_{eff,3}^{(3)}} A_3 |A_3|^2 \quad (14)$$

$$\frac{\partial A_4}{\partial z} + \beta_{14} \frac{\partial A_4}{\partial t} + \frac{i}{2} \beta_{24} \frac{\partial^2 A_4}{\partial t^2} + \frac{1}{2} \alpha_4 A_4 = i\gamma \left[\left(|A_4|^2 + 2 \sum_{k \neq 4} |A_k|^2 \right) A_4 + 2A_3^* A_1 A_2 e^{-i\Delta kz} \right] - \frac{\alpha_{0,4}}{2A_{eff,4}^{(3)}} A_4 |A_4|^2 \quad (15)$$

After rearranging the equation, we obtain the following form:

$$\frac{\partial A_1}{\partial z} = i\gamma \left[\left(|A_1|^2 + 2 \sum_{k \neq 1} |A_k|^2 \right) A_1 + 2A_2^* A_3 A_4 e^{i\Delta kz} \right] - \beta_{11} \frac{\partial A_1}{\partial t} - \frac{i}{2} \beta_{21} \frac{\partial^2 A_1}{\partial t^2} - \frac{1}{2} \alpha_1 A_1 - \frac{\alpha_{0,1}}{2A_{eff,1}^{(3)}} A_1 |A_1|^2 \quad (16)$$

$$\frac{\partial A_2}{\partial z} = i\gamma \left[\left(|A_2|^2 + 2 \sum_{k \neq 2} |A_k|^2 \right) A_2 + 2A_1^* A_3 A_4 e^{i\Delta kz} \right] - \beta_{12} \frac{\partial A_2}{\partial t} - \frac{i}{2} \beta_{22} \frac{\partial^2 A_2}{\partial t^2} - \frac{1}{2} \alpha_2 A_2 - \frac{\alpha_{0,2}}{2A_{eff,2}^{(3)}} A_2 |A_2|^2 \quad (17)$$

$$\frac{\partial A_3}{\partial z} = i\gamma \left[\left(|A_3|^2 + 2 \sum_{k \neq 3} |A_k|^2 \right) A_3 + 2A_4^* A_1 A_2 e^{-i\Delta kz} \right] - \beta_{13} \frac{\partial A_3}{\partial t} - \frac{i}{2} \beta_{23} \frac{\partial^2 A_3}{\partial t^2} - \frac{1}{2} \alpha_3 A_3 - \frac{\alpha_{0,3}}{2A_{eff,3}^{(3)}} A_3 |A_3|^2 \quad (18)$$

$$\frac{\partial A_4}{\partial z} = i\gamma \left[\left(|A_4|^2 + 2 \sum_{k \neq 4} |A_k|^2 \right) A_4 + 2A_3^* A_1 A_2 e^{-i\Delta kz} \right] - \beta_{14} \frac{\partial A_4}{\partial t} - \frac{i}{2} \beta_{24} \frac{\partial^2 A_4}{\partial t^2} - \frac{1}{2} \alpha_4 A_4 - \frac{\alpha_{0,4}}{2A_{eff,4}^{(3)}} A_4 |A_4|^2 \quad (19)$$

2.4 Degenerate FWM Coupled Amplitude Equations

When the two pump frequencies coincide such that $\omega_1 = \omega_2$, degenerate FWM is in play. We now have the following governing coupled-amplitude equations:

$$\frac{\partial A_1}{\partial z} = i\gamma \left[\left(|A_1|^2 + 2 \sum_{k \neq 1} |A_k|^2 \right) A_1 + 2A_1^* A_3 A_4 e^{i\Delta kz} \right] - \beta_{11} \frac{\partial A_1}{\partial t} - \frac{i}{2} \beta_{21} \frac{\partial^2 A_1}{\partial t^2} - \frac{1}{2} \alpha_1 A_1 - \frac{\alpha_{0,1}}{2A_{eff,1}^{(3)}} A_1 |A_1|^2 \quad (20)$$

$$\frac{\partial A_3}{\partial z} = i\gamma \left[\left(|A_3|^2 + 2 \sum_{k \neq 3} |A_k|^2 \right) A_3 + 2A_4^* A_1 A_1 e^{-i\Delta kz} \right] - \beta_{13} \frac{\partial A_3}{\partial t} - \frac{i}{2} \beta_{23} \frac{\partial^2 A_3}{\partial t^2} - \frac{1}{2} \alpha_3 A_3 - \frac{\alpha_{0,3}}{2A_{eff,3}^{(3)}} A_3 |A_3|^2 \quad (21)$$

$$\frac{\partial A_4}{\partial z} = i\gamma \left[\left(|A_4|^2 + 2 \sum_{k \neq 4} |A_k|^2 \right) A_4 + 2A_3^* A_1 A_1 e^{-i\Delta kz} \right] - \beta_{14} \frac{\partial A_4}{\partial t} - \frac{i}{2} \beta_{24} \frac{\partial^2 A_4}{\partial t^2} - \frac{1}{2} \alpha_4 A_4 - \frac{\alpha_{0,4}}{2A_{eff,4}^{(3)}} A_4 |A_4|^2 \quad (22)$$

The indices 1, 3, and 4 correspond to the degenerate pump amplitude, signal amplitude, and idler amplitude, respectively.

If we ignore the effects of dispersion for a simplified model, we have the following set of coupled-amplitude equations:

$$\frac{\partial A_1}{\partial z} = i\gamma \left[\left(|A_1|^2 + 2 \sum_{k \neq 1} |A_k|^2 \right) A_1 + 2A_1^* A_3 A_4 e^{i\Delta kz} \right] - \frac{1}{2} \alpha_1 A_1 - \frac{\alpha_{0,1}}{2A_{eff,1}^{(3)}} A_1 |A_1|^2 \quad (23)$$

$$\frac{\partial A_3}{\partial z} = i\gamma \left[\left(|A_3|^2 + 2 \sum_{k \neq 3} |A_k|^2 \right) A_3 + 2A_4^* A_1 A_1 e^{-i\Delta kz} \right] - \frac{1}{2} \alpha_3 A_3 - \frac{\alpha_{0,3}}{2A_{eff,3}^{(3)}} A_3 |A_3|^2 \quad (24)$$

$$\frac{\partial A_4}{\partial z} = i\gamma \left[\left(|A_4|^2 + 2 \sum_{k \neq 4} |A_k|^2 \right) A_4 + 2A_3^* A_1 A_1 e^{-i\Delta k z} \right] - \frac{1}{2} \alpha_4 A_4 - \frac{\alpha_{0,4}}{2A_{eff,4}^{(3)}} A_4 |A_4|^2 \quad (25)$$

3 Four-wave Mixing Numerical Solver Specifications

3.1 Simulation Parameters

The following parameters are specified in order to run the simulation:

1. Pump 1 and Pump 2 Power
2. Refractive Index Models for Pump 1, Pump 2, Signal, and Idler (TE or TM Mode)
3. Pump 1, Pump 2, and Signal wavelengths
4. Pump 1, Pump 2, Signal, and Idler Linear Loss Parameters
5. Pump 1, Pump 2, Signal, and Idler Effective Self-phase Modulation Parameter
6. Pump 1, Pump 2, Signal, and Idler Two-photon Absorption Parameters
7. Pump 1, Pump 2, Signal, and Idler T_0 (FWHM/1.665)
8. Laser Repetition Rate
9. Device Length
10. Number of Periods
11. Number of Steps Along t
12. Number of Iterations Per Material
13. Number of Steps Along z-direction
14. Step Length Along t
15. Pump 1, Pump 2, Signal, and Idler Third-Order Effective Area
16. Pump 1, Pump 2, Signal, and Idler Pulse Shape

3.2 Simulation Structure

The simulation utilizes three primary MATLAB scripts: `step4_wave.m`, `PIA_Gain.m`, and `simulation_scan_4wave.m`. `step4_wave.m` handles most of the numerical computation, while `PIA_Gain.m` sets up the entirety of the simulation including parameters and plotting. `simulation_scan_4wave.m` is used for scanning between a range of signal wavelengths in order to find the phase-matching point by using `PIA_Gain.m` in combination with `step4_wave.m`.

3.3 Split-Step Fourier Method (SSFM)

The `step4_wave.m` function utilizes the split-step method for solving the nonlinear Schrödinger equations.

We can now express the coupled-amplitude equations in the following form:

$$\frac{\partial A_1}{\partial z} = (\hat{D}_1 + \hat{N}_1)A_1 \quad (26)$$

$$\frac{\partial A_2}{\partial z} = (\hat{D}_2 + \hat{N}_2)A_2 \quad (27)$$

$$\frac{\partial A_3}{\partial z} = (\hat{D}_3 + \hat{N}_3)A_3 \quad (28)$$

$$\frac{\partial A_4}{\partial z} = (\hat{D}_4 + \hat{N}_4)A_4 \quad (29)$$

\hat{D}_i for $i = 1, 2, 3, 4$ and \hat{N}_i for $i = 1, 2, 3, 4$ are the differential operator accounting for dispersion and nonlinear operator governing the effects of fibre nonlinearities, respectively [3]. Each of these operators are specified as follows:

$$\hat{D}_i = -\beta_{1i} \frac{\partial}{\partial t} - \frac{i}{2} \beta_{2i} \frac{\partial^2}{\partial t^2} - \frac{1}{2} \alpha_i \quad (30)$$

$$\hat{N}_i = i\gamma |A_i|^2 + 2i\gamma \frac{A_j^* A_k A_l e^{i\Delta k z}}{A_i} - \frac{\alpha_{0,i}}{2A_{eff,i}^{(3)}} |A_i|^2 \quad (31)$$

The numerical solver computes the first linear half-step (dispersion), followed by the nonlinear step and the second linear half-step. For the nonlinear half-step, a 4th-order Runge Kutta algorithm is used.

4 Non-degenerate FWM Simulation Results

4.1 Non-degenerate FWM Signal Wavelength Scan

A scan with the following parameters was conducted for the non-degenerate FWM process. The signal wavelengths ranged from 1100 nm to 1600 nm.

1. Pump 1 and Pump 2 Power: 30 mW, 40 mW, 50 mW, 60 mW
2. Refractive Index Models for Pump 1, Pump 2, Signal, and Idler: TE, TM, TE, TM
3. Pump 1, Pump 2, and Signal wavelengths: 1310 nm, 1310 nm, 1100 nm - 1600 nm
4. Pump 1, Pump 2, Signal, and Idler Linear Loss Parameters: 200 m^{-1} , 200 m^{-1} , 200 m^{-1} , 200 m^{-1}
5. Pump 1, Pump 2, Signal, and Idler Effective Self-phase Modulation Parameter: $100 \times 10^{-20} \frac{\text{m}^2}{\text{W}}$, $100 \times 10^{-20} \frac{\text{m}^2}{\text{W}}$, $100 \times 10^{-20} \frac{\text{m}^2}{\text{W}}$, $100 \times 10^{-20} \frac{\text{m}^2}{\text{W}}$

6. Pump 1, Pump 2, Signal, and Idler Two-photon Absorption Parameters: $1.5 \times 10^{-12} \frac{\text{m}}{\text{W}}$, $1.5 \times 10^{-12} \frac{\text{m}}{\text{W}}$, $1.5 \times 10^{-12} \frac{\text{m}}{\text{W}}$, $1.5 \times 10^{-12} \frac{\text{m}}{\text{W}}$
7. Pump 1, Pump 2, Signal, and Idler T_0 (FWHM/1.665): $3.867 \times 10^{-14} \text{ s}$, $3.867 \times 10^{-14} \text{ s}$, $3.867 \times 10^{-12} \text{ s}$, $3.867 \times 10^{-12} \text{ s}$
8. Laser Repetition Rate: 80 MHz
9. Device Length: 1 mm
10. Number of Periods: 100
11. Number of Steps Along t : 1023
12. Number of Iterations Per Material: 5
13. Number of Plots in z-direction: 101
14. Step Length Along t : $5.859375 \times 10^{-14} \text{ s}$
15. Pump 1, Pump 2, Signal, and Idler Third-Order Effective Area: $1 \times 10^{-12} \text{ m}^2$, $1 \times 10^{-12} \text{ m}^2$, $1 \times 10^{-12} \text{ m}^2$, $1 \times 10^{-12} \text{ m}^2$
16. Pump 1, Pump 2, Signal, and Idler Pulse Shape: Sech, Sech, Exponential, Exponential

The gain profiles as a function of signal wavelength for non-degenerate FWM at 30 mW, 40 mW, 50 mW, and 60 mW are shown in Figure 1. The gain profiles display two broad peaks near 1250 nm and 1380 nm.

4.2 Non-degenerate FWM - Changing Pump Power

At a signal wavelength of 1380 nm, the signal gain as a function of device length has been plotted at six different values for pump power: 30 mW, 40 mW, 50 mW, 60 mW, 70 mW, and 80 mW. The plots are shown in Figure 2.

4.3 Non-degenerate FWM - Changing Two-photon Absorption Coefficient

At a signal wavelength of 1380 nm, the signal gain as a function of device length has been plotted at four different values for two-photon absorption coefficient: $1.5 \times 10^{-12} \frac{\text{m}}{\text{W}}$, $2.0 \times 10^{-12} \frac{\text{m}}{\text{W}}$, $2.5 \times 10^{-12} \frac{\text{m}}{\text{W}}$, and $3.0 \times 10^{-12} \frac{\text{m}}{\text{W}}$. The plots are shown in Figure 3.

As can be seen in the figure, the overall gain of the device is highly sensitive to changes in the two-photon absorption coefficient. This is an interesting observation as two-photon absorption is a phenomenon that only occurs in semiconductor devices. Even a two-fold increase in the TPA coefficient will lead to a decrease in signal gain from 90 dB to 50 dB. This observation is consistent with the findings by Peng Xie et al., where the intensities of signal output with TPA and free-carrier effects at 0.2 W to 1 W are consistently lower than those without the effects of TPA [5].

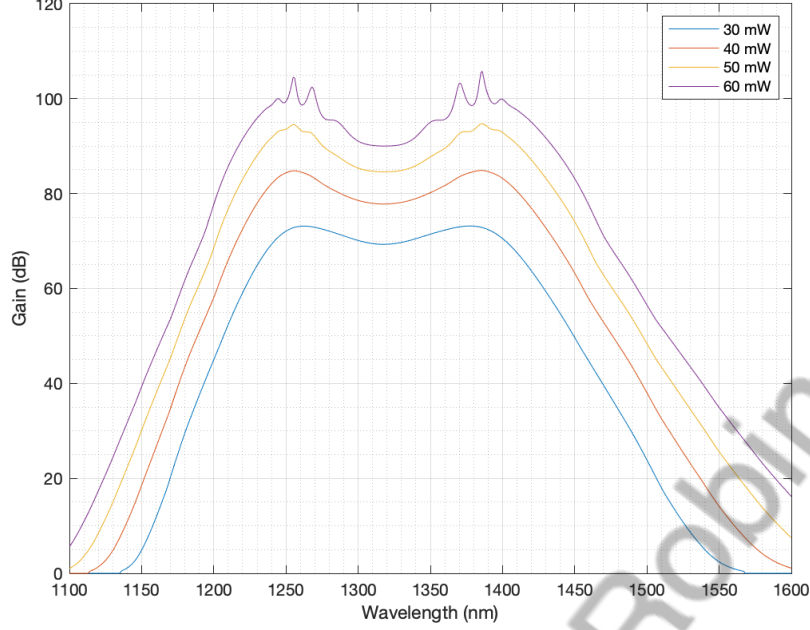


Figure 1: Gain Profile for non-degenerate FWM at 30 mW, 40 mW, 50 mW, and 60 mW Pump Power. As the pump power increases, both the maximum gain and the width of the gain profiles increase [4]. At all of the pump powers, two broad gain peaks near 1250 nm and 1380 nm are seen.

5 Degenerate FWM Simulation Results

5.1 Non-degenerate FWM Signal Wavelength Scan

A scan with the following parameters was conducted for the degenerate FWM process. The signal wavelengths ranged from 1100 nm to 1600 nm.

1. Pump Power: 30 mW, 40 mW, 50 mW, 60 mW
2. Refractive Index Models for Pump, Signal, and Idler: TE, TM, TM
3. Pump and Signal wavelengths: 1310 nm, 1100 nm - 1600 nm
4. Pump, Signal, and Idler Linear Loss Parameters: 200 m^{-1} , 200 m^{-1} , 200 m^{-1}
5. Pump, Signal, and Idler Effective Self-phase Modulation Parameter: $100 \times 10^{-20} \frac{\text{m}^2}{\text{W}}$, $100 \times 10^{-20} \frac{\text{m}^2}{\text{W}}$, $100 \times 10^{-20} \frac{\text{m}^2}{\text{W}}$
6. Pump, Signal, and Idler Two-photon Absorption Parameters: $1.5 \times 10^{-12} \frac{\text{m}}{\text{W}}$, $1.5 \times 10^{-12} \frac{\text{m}}{\text{W}}$, $1.5 \times 10^{-12} \frac{\text{m}}{\text{W}}$
7. Pump, Signal, and Idler T_0 (FWHM/1.665): $3.867 \times 10^{-14} \text{ s}$, $3.867 \times 10^{-12} \text{ s}$, $3.867 \times 10^{-12} \text{ s}$
8. Laser Repetition Rate: 80 MHz

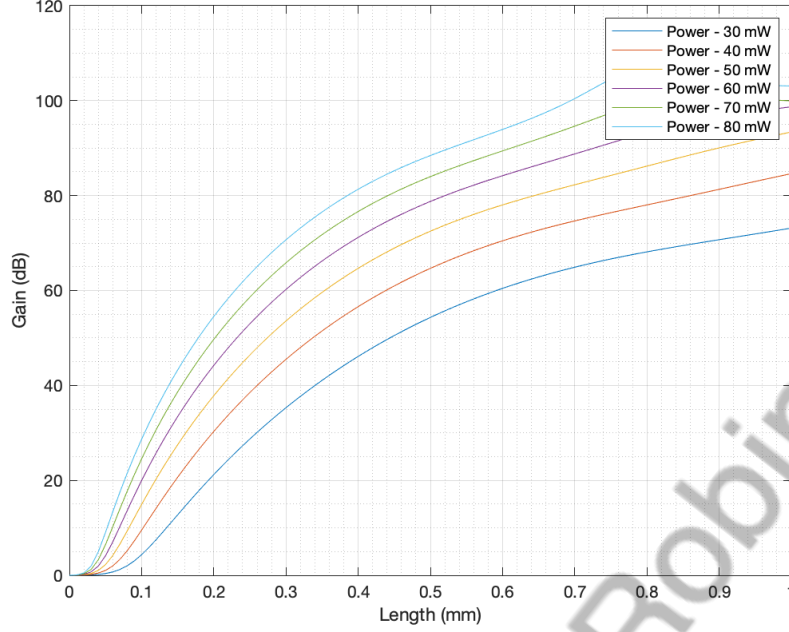


Figure 2: Gain as a function of device length for non-degenerate FWM (1380 nm Signal Wavelength) at 30 mW, 40 mW, 50 mW, 60 mW, 70 mW, and 80 mW Pump Power. As the pump power increases, the overall gain at the end of the device increases as well. In addition, the rate of change of the signal gain with respect to device length is much higher at 80 mW than it is at 30 mW.

9. Device Length: 1 mm
10. Number of Periods: 100
11. Number of Steps Along t : 1023
12. Number of Iterations Per Material: 5
13. Number of Plots in z-direction: 101
14. Step Length Along t : 5.859375×10^{-14} s
15. Pump, Signal, and Idler Third-Order Effective Area: 1×10^{-12} m², 1×10^{-12} m², 1×10^{-12} m²
16. Pump, Signal, and Idler Pulse Shape: Sech, Exponential, Exponential

The gain profiles as a function of signal wavelength for degenerate FWM at 30 mW, 40 mW, 50 mW, and 60 mW are shown in Figure 4. The gain profiles display two broad peaks near 1150 nm and 1500 nm.

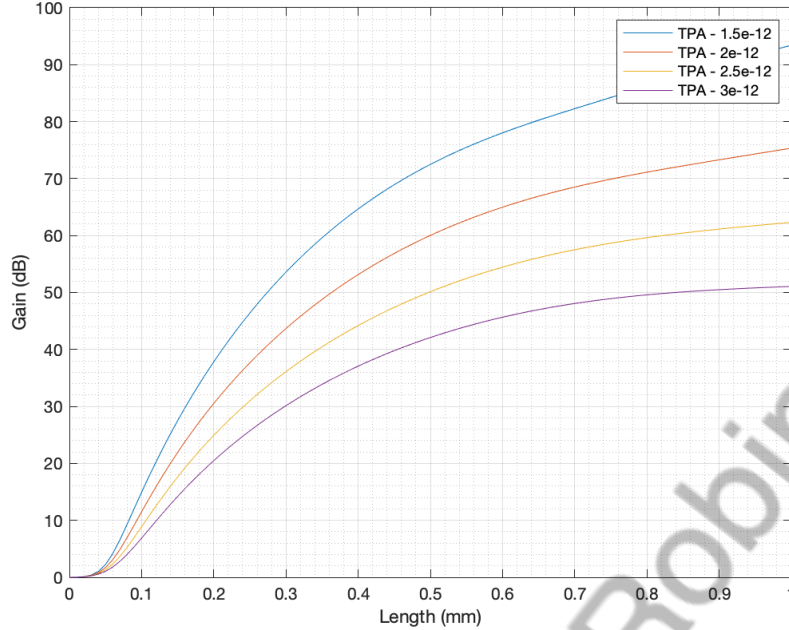


Figure 3: Gain as a function of device length for non-degenerate FWM (1380 nm Signal Wavelength) at the following values for two-photon absorption: $1.5 \times 10^{-12} \frac{\text{m}}{\text{W}}$, $2.0 \times 10^{-12} \frac{\text{m}}{\text{W}}$, $2.5 \times 10^{-12} \frac{\text{m}}{\text{W}}$, and $3.0 \times 10^{-12} \frac{\text{m}}{\text{W}}$. When the TPA coefficient is increased by a factor of two, the signal gain has decreased from 90 dB to 50 dB.

5.2 Degenerate FWM - Changing Pump Power

At a signal wavelength of 1500 nm, the signal gain as a function of device length has been plotted at six different values for pump power: 30 mW, 40 mW, 50 mW, 60 mW, 70 mW, and 80 mW. The plots are shown in Figure 5.

5.3 Degenerate FWM - Changing Two-photon Absorption Coefficient

At a signal wavelength of 1500 nm, the signal gain as a function of device length has been plotted at four different values for two-photon absorption coefficient: $1.5 \times 10^{-12} \frac{\text{m}}{\text{W}}$, $2.0 \times 10^{-12} \frac{\text{m}}{\text{W}}$, $2.5 \times 10^{-12} \frac{\text{m}}{\text{W}}$, and $3.0 \times 10^{-12} \frac{\text{m}}{\text{W}}$. The plots are shown in Figure 6.

As can be seen in the figure, the overall gain of the device is highly sensitive to changes in the two-photon absorption coefficient. Even a two-fold increase in the TPA coefficient will lead to a decrease in peak signal gain from 90 dB to 45 dB.

6 Conclusion and Discussion

In this study, we have investigated the following effects for both the degenerate and non-degenerate processes: (i) changing the pump power on the gain spectrum (gain as a function of signal wavelength), (ii) changing the pump power on the gain profile (gain as a function of device length), and

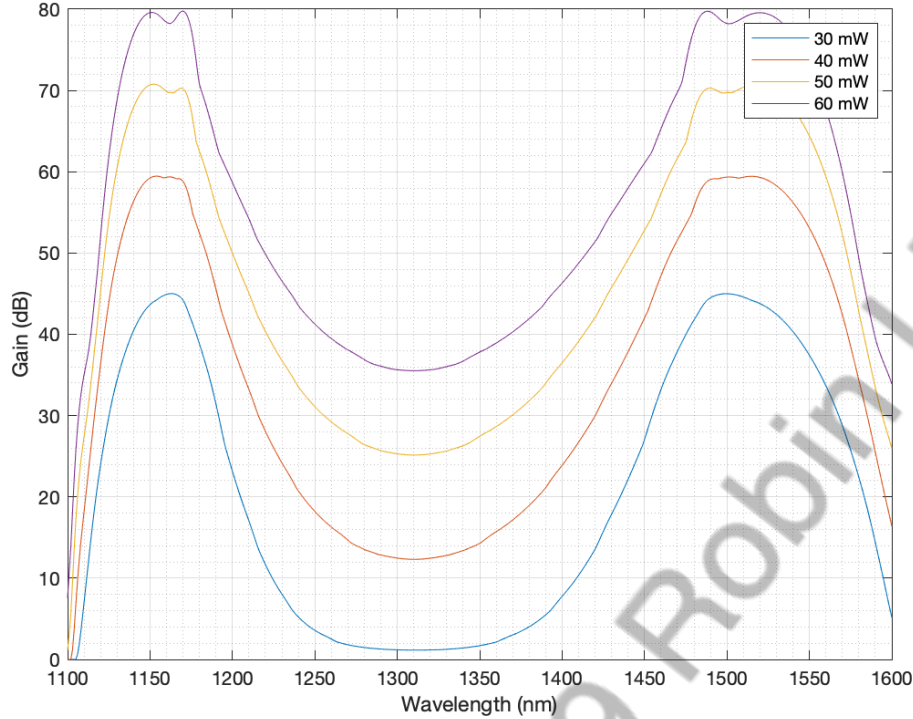


Figure 4: Gain Profile for degenerate FWM at 30 mW, 40 mW, 50 mW, and 60 mW Pump Power. At all the pump powers, the gain profiles display two broad peaks near 1150 nm and 1500 nm.

(iii) changing the two-photon absorption on the gain profile (gain as a function of device length).

We have found that for experimentation (i), increasing the pump power increases both the width of the gain spectrum as well as the maximum gain, while the phase-matching points are approximately constant. For experimentation (ii), increasing the pump power increases the gain at the end of the device as well as the steepness of the gain profile near the front of the device. For experimentation (iii), increasing the two-photon absorption coefficient significantly decreases the gain at the end of the device.

For the non-degenerate process (pump wavelength at 1310 nm), the phase-matching wavelengths are: 1250 nm and 1380 nm. For the degenerate process (pump wavelength at 1310 nm), the phase-matching wavelengths are: 1150 nm and 1500 nm.

References

- [1] JAC Weideman and BM Herbst. Split-step methods for the solution of the nonlinear schrödinger equation. *SIAM Journal on Numerical Analysis*, 23(3):485–507, 1986.
- [2] Govind P Agrawal. Nonlinear fiber optics. In *Nonlinear Science at the Dawn of the 21st Century*, pages 195–211. Springer, 2000.

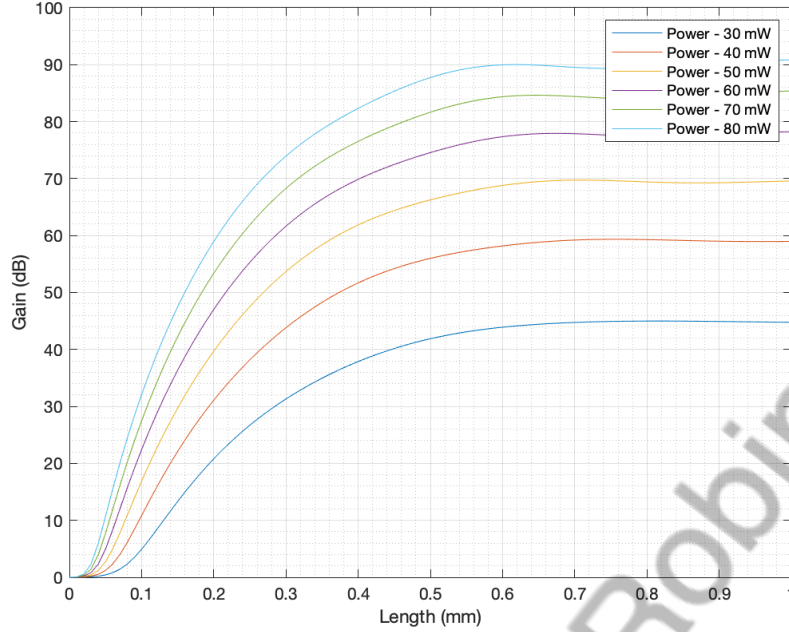


Figure 5: Gain as a function of device length for degenerate FWM (1500 nm Signal Wavelength) at 30 mW, 40 mW, 50 mW, 60 mW, 70 mW, and 80 mW Pump Power

- [3] Oleg V Sinkin, Ronald Holzlohner, John Zweck, and Curtis R Menyuk. Optimization of the split-step fourier method in modeling optical-fiber communications systems. *Journal of light-wave technology*, 21(1):61–68, 2003.
- [4] Seyedeh Bentolhoda Nazemosadat Arsanjani. *Applications of four-wave mixing and cross phase modulation in highly nonlinear fibers*. PhD thesis, 2012.
- [5] Peng Xie, Qibing Sun, Leiran Wang, Yu Wen, Xinyu Wang, Guoxi Wang, Chao Zeng, Mu-long Liu, Zhiqiang Ge, and Zhizhou Lu. Impact of two-photon absorption and free-carrier effects on time lens based on four-wave mixing in silicon waveguides. *Applied Physics Express*, 11(8):082204, 2018.

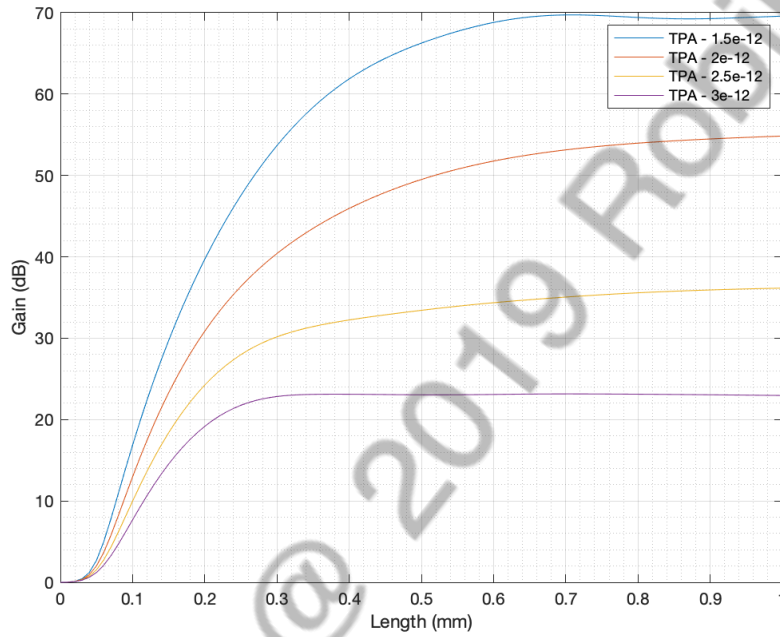


Figure 6: Gain as a function of device length for degenerate FWM (1500 nm Signal Wavelength) at the following values for two-photon absorption: $41.5 \times 10^{-12} \frac{\text{m}}{\text{W}}$, $2.0 \times 10^{-12} \frac{\text{m}}{\text{W}}$, $2.5 \times 10^{-12} \frac{\text{m}}{\text{W}}$, and $3.0 \times 10^{-12} \frac{\text{m}}{\text{W}}$.